HAL
open science

Metallic impurity sources behavior during ICRH in EAST

Guillaume Urbanczyk, X.J. Zhang, L. Colas, A. Ekedahl, S. Heuraux, J. G. Li, C.M. M Qin, Y.P. Zhao, L. Zhang, X.D. D Yang

▶ **To cite this version:**

Guillaume Urbanczyk, X.J. Zhang, L. Colas, A. Ekedahl, S. Heuraux, et al.. Metallic impurity sources behavior during ICRH in EAST. Nuclear Materials and Energy, 2018, 17, pp.274-278. 10.1016/j.nme.2018.10.008 . cea-02265780

HAL Id: cea-02265780

https://cea.hal.science/cea-02265780v1

Submitted on 12 Aug 2019

HAL is a multi-disciplinary open access archive for the deposit and dissemination of scientific research documents, whether they are published or not. The documents may come from teaching and research institutions in France or abroad, or from public or private research centers.

L'archive ouverte pluridisciplinaire **HAL**, est destinée au dépôt et à la diffusion de documents scientifiques de niveau recherche, publiés ou non, émanant des établissements d'enseignement et de recherche français ou étrangers, des laboratoires publics ou privés.

Metallic impurity sources behavior during ICRH in EAST

G. Urbanczyk[a,b], X.J. Zhang[b], L. Colas[a], A. Ekedahl[a], S. Heuraux[c], J.G. Li[b], C.M. Qin[b], Y.P. Zhao[b], L. Zhang[b], X.D. Yang[b]

[a] *CEA, IRFM, F-13108 Saint Paul-Lez-Durance, France.*
[b] *Institute of Plasma Physics, Chinese Academy of Sciences, Hefei 230031, People's Republic of China*
[c] *Université de Lorraine-CNRS UMR 7198 BP 70239 FST_IJL F-54506 Vandoeuvre*

guillaume.urbanczyk@cea.fr

Abstract.

High-Z impurities production is often observed during Ion Cyclotron Range of Frequencies (ICRF) waves' injection, which are likely due to RF sheath formation on Plasma Facing Components (PFCs). Based on Extreme UV (EUV) spectrometry data, this study takes profit from the diversity of materials in the Experimental Advanced Superconducting Tokamak (EAST) to extract local information on plasma-surface interactions during ICRH (Ion Cyclotron Resonance Heating). Intensities of the different spectral lines normalized to line-integrated plasma density, exhibit different parametric dependencies over scans of ICRH and LH (Lower Hybrid) power and for different toroidal phasing between straps. Materials close and magnetically-connected to an active antenna tend to show better correlation with ICRF parameters – such as power and feeding scheme – than those which are far away or not connected. ICRF phasing however did not have significant influence on impurity sources, probably due to the absence of feedback control. It is further shown that the plasma content in impurities from divertor region (W line intensity) better correlates with the total injected power rather than with ICRF power.

1. Introduction.

In view of future experiments on larger devices like ITER and CFETR, the Experimental Advanced Superconducting Tokamak (EAST) aims at long pulses at high power in steady state. Higher power demand nevertheless comes with challenges in terms of plasma surface interaction and impurity mitigation. Methods for optimizing high power scenarios using more of the 12MW ICRF power available at the generator depend a priori on where the impurities are produced, and on which physical mechanism is at play for their production. This study specifically investigates impurity production issues in discharges with ICRH in EAST, depending on their spatial origin in the vacuum chamber.

As ICRF wave coupling can be quite poor in EAST [1], on top of thermal sheath present on any PFC intercepting a magnetic flux tube, RF sheaths form and are known for enhancing interactions particularly at proximity of antennas due to strong near-fields. This is also true further away to a smaller extent, and sometimes even in non-magnetically connected regions due to far-field [2] as observed on many devices like Tore Supra [3] [4], Alcator C-Mod [5] [6] [7], JET [8], ASDEX Upgrade [9] or LAPD [10]. ICRF wave absorption efficiency – estimated with combining break-in-slope technique with ITER89-P scaling law [11] – is believed to be of the order of 35%, therefore a significant part of unabsorbed power might as well lead to far-field-induced interactions in unexpected locations, motivating the need to localize and characterize impurity sources at least qualitatively [12] [13]. One difficulty of the this study comes from the lack of appropriate edge diagnostic to characterize impurities sources, like visible spectroscopy [14] [8], meaning that high-Z impurities can in EAST only be seen in the core using an Extreme UltraViolet (EUV) spectrometer [15] [16]. The present study proposes to take profit from the diversity of materials in EAST to extract local information on plasma-surface interaction. Even if we mostly focus on the characterization of ICRF-related sources of impurities, a secondary objective is also to identify dominant mechanisms in different regions. Titanium was also added in a precise and unique location to serve as trace of plasma-material interactions in a specific area. The first section introduces the experimental

protocol before discussing the influence of magnetic connections, RF power and phasing on impurities presumably produced from different regions.

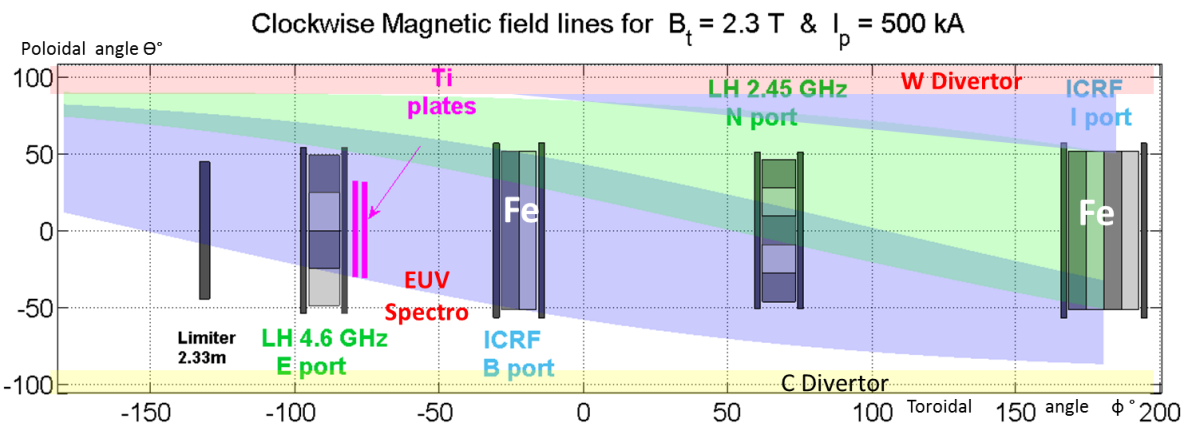

Figure 1. Toroidal-Poloidal (ϕ-Θ) 2D map of EAST showing magnetic connections between objects, materials, heating systems and EUV spectrometer, seen from center of the torus.

2. Experimental conditions and protocol in EAST.

EAST is a superconducting tokamak equipped with two divertors allowing double null, lower (LSN) and upper single null (USN) configurations with following parameters of this study: toroidal magnetic field Bt≈2.3T, plasma current Ip≈500kA, major radius Ro≈1.85m, minor radius a≈0.44m, triangularity $\delta \approx 0.5$ and elongation $\kappa \approx 1.65$. Plasma isotopic ratio (H/H+D) rarely decreasing below 5% in EAST, strong lithium coating is daily applied before each session mainly to keep low-Z impurity like oxygen and carbon down to acceptable levels in terms of radiated power. Lithium can however also have mitigating effects on high-Z impurity contamination like tungsten [17], which effect changes along the experiments as Li is eroded and redeposited elsewhere. This can make comparison of data from different days and hour less consistent, so that we group cases in series of shots during same days. In this study all plasmas were in L-mode and USN configurations. Auxiliary heating systems include two Lower Hybrid Current Drive (LHCD) grills located in E-port (4.6 GHz and $2<n_{\|}<3$) and N-port (2.45 GHz and $1.8<n_{\|}<2.5$) [18], and two ICRF antennas heating hydrogen minority in deuterium plasmas, the one is located in B-port (31.5 MHz) and composed of two arrays of two straps and the other is located in I-port (35 MHz) and composed of an array of four straps (Fig. 1) [1, 2, 18]. When not mentioned, all straps in a given antenna were fed with RF currents of comparable magnitude. The phase difference between RF currents in toroidally-adjacent straps was set at 180° ("dipole phasing"), but is not feedback-controlled.

Using a EUV spectrometer [20], the brightness of various high-Z impurities lines (20Å to 150Å) was investigated with wavelength resolution defined as full width at half maximum of about 0.22-0.3Å and at 100-200Å respectively. These brightness values mostly emitted from plasma core are systematically normalized by line-integrated plasma density, and their parametric variations from pulse to pulse within the same experimental session are interpreted as a change in the sources of impurities rather than their transport. This assumption is fairly good for most species which radiate relatively close to the edge and easily penetrate inside plasma. Note this can be questionable for tungsten coming from divertor region, as it is not only expected to be better screened and moreover whose emissivity mainly comes from plasma center, therefore more sensitive to transport in both SOL and confined plasma. As far as edge turbulent transport is concerned, it was shown both in Alcator C-Mod and that it does not change much in presence of ICRH [21, 22] and neither did electron temperature (<10%).

Ions	λ (Å)	Te (keV)	ρ
Ti^{17+}	144.76	0.6	< 0.7
Fe^{21+}	132.85	1.98	< 0.6
W^{45+}	126.99	4	< 0.2
Wuta=$W^{28->46}$	45->70	3 → 6	< 0.85

Table 1. Spectral lines observed by EUV spectrometer in the present study with the corresponding emitted wavelength λ, minimal temperature T_e and normalized radius ρ at which ionization occur

Different lines, corresponding to different materials summarized under Table 1 are seen as footprints of plasma-material interaction in a relatively precise location on the inner surface of the device; Iron is found on antenna Faraday screens (underneath a boron carbide coating), and upper divertor is made of tungsten (noted W for W_{UTA}, which is an average of all spectral lines from W^{27+} until W^{45+}). In addition, two titanium passive plates were installed on purpose at one toroidal location of the outer midplane to serve as impurity trace (ϕ ~ -90° and -30° < Θ < 30°). Titanium was found appropriate mainly for three reasons; a spectral line could easily be distinguished with EUV spectrometer from those of others species present in EAST, it can be used as a permanent plasma facing component without affecting the vacuum conditions and its cost is reasonably low.

The blue region in Fig. 1 shows that only B-port ICRF antenna is magnetically connected to the Ti plates. Such location was chosen to confirm the role of magnetic connections in RF sheaths formation [23] and ICRH-enhanced plasma-surfaces interactions. In the following, the different spectral lines are monitored over scans of ICRF and LH power by several combinations of both antennas, with several toroidal phasing between straps.

3. Role of magnetic connection to the active RF antenna

The objective of the following series of shots is to provide a first picture on how different species behave according to the magnetic connections of the different plasma-facing materials with active ICRF antennas. Two different scenarios are preliminary discussed to assess materials dependences on any physical effects, before trying to conclude on ICRF-related ones. Black curves in Fig. 2 provide levels of impurities in a typical discharge only heated with 1.4MW LH power while red curves stand for a case when B-port and I-port ICRF antennas were also powered successively in dipole phasing and with 5Hz power modulations between 0.5 and 1MW as shown in graph 2d. All metal impurity signals increase fairly similarly during application of LH power. When the ICRF antennas are activated, Ti and Fe contents in the plasma increase in magnitude and react to power modulations visible on both signals. As the Fe and Ti-covered objects are both magnetically connected to B-port antenna, strongest interactions occurred when this antenna was active. Fe is also well connected to the I-port antenna, so we would expect similar levels in both cases, but as B-port antenna is much smaller, higher power densities are expected for same antenna loading and power. Finally W seems to react to both ICRH and LH power. In the following sections are discussed the impurities dependences with ICRF power and phasing.

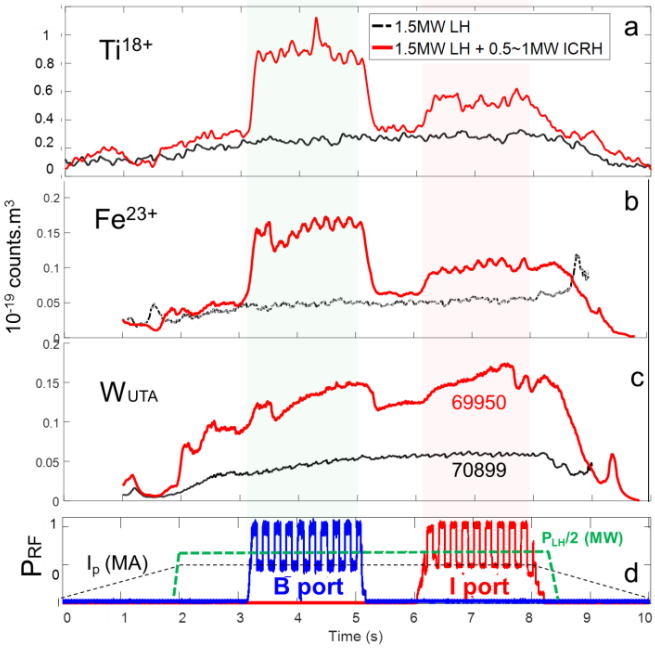

Figure 2. Time traces of spectral lines brightness from EUV spectrometer normalized by line-integrated density for; Ti XVIII (a), Fe XXIII (b), W (c), for EAST ohmic pulse #70899 and RF heated pulse #69950

4. Impurity correlation with ICRF power.

To study metallic impurity behavior with ICRF power, three series of shots with both antennas powered together and scans of total ICRF power $P_{ICRF} = P_I + P_B = 2\ P_I$ at generator and different conditions were analyzed. From Fig. 2, we know that P_{ICRF} is not a fully relevant parameter in itself to estimate impurity levels as power from I (P_I) and B ports (P_B) have different influence on different impurities. It consequently matters to have a relatively constant ratio P_I/P_B over power scan, which is kept close to unity ($P_I \approx P_B$). EUV spectral lines intensities were systematically normalized to line-integrated density from interferometer and averaged over small periods of time (between 0.02 and 0.1s) and noted *Imp*. For each species and shot, ICRF-related impurity production Y_{shot} is calculated as $Y_{shot} = (Imp_{withIC} - Imp_{withoutIC}) / \max(Imp_{withIC} - Imp_{withoutIC})_{over.all.shots}$ and represented in Fig. 3. In the blue series only P_{ICRF} increased, while in the black series P_{ICRF} increased together with P_{LH}. In the red series, power balance on B-port antenna straps is changed over the scan: one of the four radiating straps is switched off as the power is increased.

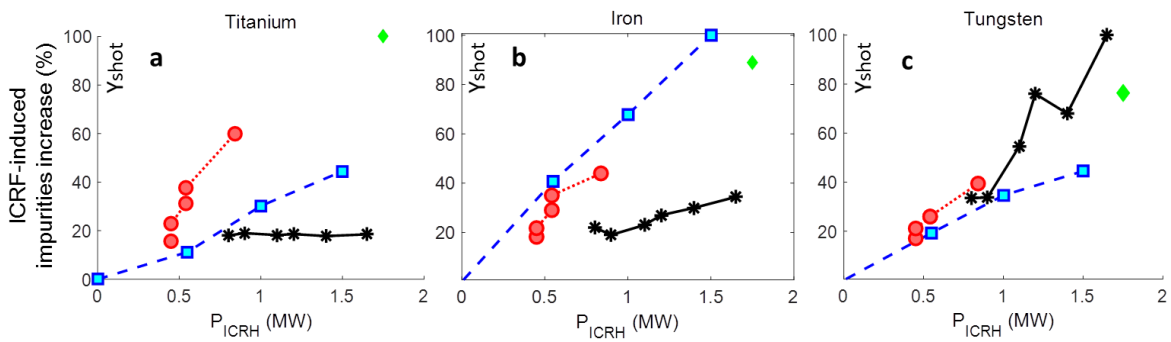

Figure 3. ICRF-related impurity production (Y_{shot}) as a function of ICRF power for (a) Ti, (b) Fe and (c) W. In the blue series, LH power remained constant while it changed in the black series. Power balance on straps was changed in the red series. Green dot corresponds to a discharge only heated with ICRF power (balanced on all straps)

Graph (a) shows that Ti is very sensitive to discharge conditions as each series behaves differently, whereas Fe and W have different behaviours but both globally increase with P_{ICRF}.

At constant LH power and same ICRF power on each strap (blue series), all impurities follow a linear trend. For a same amount of ICRF power on straps, we observe much higher titanium content when it is unbalanced (red series) than when it is balanced (blue series). On the contrary for tungsten, red and blue series follow similar evolutions with P_{ICRF}, suggesting that divertor region is insensitive to the antenna settings and only depend on the power injected. Furthermore looking at the cases when ICRH increases together with LH power (black series), W content increases strongly hinting that divertor region is sensitive to the total power injected rather than ICRH power alone. Ti on the contrary remains constant, showing that interactions in regions closely connected to B-port antenna may not only depend on ICRH power but also on how it is launched (antenna design, power balance on straps). Iron from antenna Faraday screens always increases with ICRH power in a similar fashion in all cases showing a generally good correlation. Fe sensitivity to one single antenna settings is however less obvious than for Ti since Fe can come from both antenna Faraday screens.

5. Impurity correlation with total injected power

Characteristic of divertor region, tungsten is badly correlated with ICRH settings. This hints that divertor region is not specifically sensitive to P_{ICRF} but to total injected power P_{TOT}, which can be confirmed by representing the impurity increase as a function of P_{TOT} for all shots (Fig. 4). Impurity increase is defined as $|Imp_{during\ IC} - Imp_{before\ IC}|$ with ICRH (red series) otherwise $|Imp_{during\ LH} - Imp_{before\ LH}|$ (black series). Tungsten concentration clearly correlates with P_{TOT}, whereas no consistent link between Fe and Ti with P_{TOT} can be established. For these two species, in the absence of ICRH, the impurity concentration is quite independent of the LH power in the range 1-2.5MW.

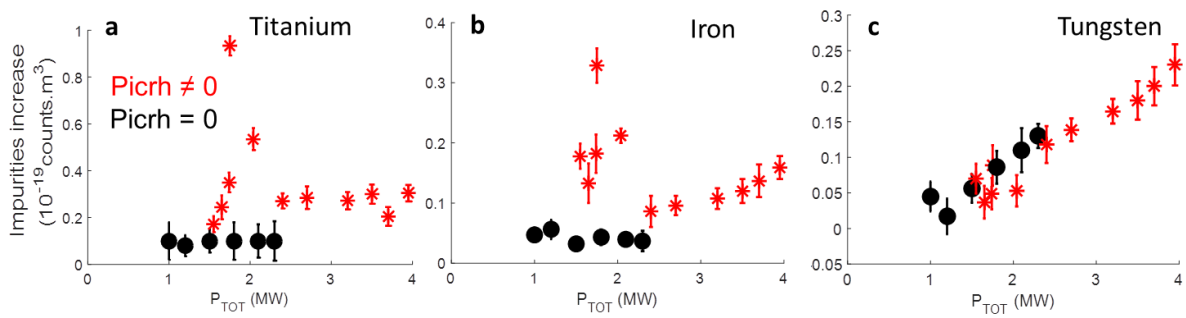

Figure 4. Normalized spectral line brightness increase as a function of total injected power for Ti (a), Fe (b) and W (c). Red and black series stand for shots with and without ICRH.

6. Impurity correlation with ICRF phasing.

The second key parameter of ICRF system to investigate is the phase difference between RF currents on toroidally adjacent straps. In EAST, only phases of I-port antenna were changed whereas B-port always operated in dipole phasing. A series of shots with same power and loadings on both antennas and different phases on I-port antenna were studied. Ti, Fe and W remained relatively insensitive to the phase variation, which is surprising as results in other devices show that impurity production generally increases as phasing tend to deviate from dipole towards monopole [24, 25]. The absence of real time feedback control of EAST ICRF phases [26] is likely to account for inconsistent observations along phase scan.

7. Discussions and prospects

By using EUV spectrometer to characterize the presence of high-Z metallic impurities in the core, and taking profit from the multiplicity of materials in EAST, we were able to deduce local information about ICRF-related plasma surface interactions. Magnetic connection between objects of specific materials and active antennas undeniably plays a role which becomes more and more complex as distance from active antenna increases. Iron from antenna Faraday Screens typically correlates well with ICRF power, which is believed to be the result of near-field enhanced interactions, so far consistent with most observations elsewhere [3, 4, 5, 6, 7, 8, 9, 10]. Rectification effects are then transported along magnetic field lines from active antenna to connected regions, as observed through the titanium content evolution when degrading the power balance on antenna straps (red series in Fig. 3a). This observation is consistent with uncompensated image currents induced on antenna limiters, leading to stronger potential rectification at the Ti plates [9]. Besides, for well-balanced power on straps, ICRH-induced rectification can be inhibited in the same region (black series in Fig. 3a). This could additionally be the result of improved wave absorption by increasing total injected power which will be discussed more in detail in a future study including wave absorption efficiency calculations. Characteristic of the divertor region, tungsten shows much better correlation with total injected power (Fig. 4c) rather than ICRF power, or settings like power balance (red series in Fig. 3c) or phasing between straps. Divertor outer target was identified in others devices to be an important source of impurities [13, 27] but not specifically due to ICRH [12, 14]. In EAST, despite evidences from divertor Langmuir probes of potential rectification [28], our results indicate that the divertor region is sensitive to total power regardless from which system and how it is injected. This suggests RF sheath play a negligible role, whereas heat fluxes on divertor target apparently matter the most, as far as these level of power are concerned. Most metallic impurities were moreover insensitive to ICRF phasing which was not feedback controlled [26]. Difficulties still arise on a poor estimation of ICRF power injected in the vessel as losses in transmission lines cannot be neglected. It should be pointed out that the two ICRF antennas have different designs and sizes, meaning that not only the magnetic connection can play a role for the impurity increase, but also the antenna design. B-port is quite systematically the principal cause of impurity production, which can be partially understood considering its smaller size compared to I-port, leading to higher power density for similar generator power and loading.

To complete the studies presented here, the titanium plate has been moved to B-port and silver plates were added to I-port so that each material is characteristic of interactions around one antenna. More information is expected from the upcoming campaign.

Acknowledgments

The whole EAST ICRH team, colleagues in charge of reciprocating probes and IRFM GMICS team are warmly acknowledged.

This work has been carried out within the framework of the EUROfusion Consortium and has received funding from the Euratom research and training program 2014-2018 under grant agreement No 633053. The views and opinions expressed herein do not necessarily reflect those of the European Commission.

This work was supported partly by National key research and development program (grant nos 2016YFA0400600 and 2016YFA0400601). This work was supported partly by National Magnetic confinement Fusion Science Program (grant nos 2015GB101001). This work was also supported partly by the National Natural Science Foundation of China under grant nos 11675213, 11375235 and 11375236.

References

[1] J.H. Zhang et al 2017 Nucl. Fusion 57 066030 (10pp)
[2] G. Urbanczyk et al EPJ Web of Conferences 157, 03057 (2017)
[3] L Colas et al. Plasma Phys. Control. Fusion 49 (2007) B35–B45
[4] M. Kubic et al. Journal of Nuclear Materials 438 (2013) S509–S512
[5] R Ochoukov et al, Plasma Phys. Control. Fusion 56 (2014) 015004
[6] I. Cziegler et al, Plasma Phys. Control. Fusion 54 (2012) 105019 (9pp)
[7] R. Hong et al. Plasma Phys. Control. Fusion 59 (2017) 105008
[8] V. Bobkov et al. Journal of Nuclear Materials 438 (2013) S160–S165
[9] V. Bobkov EPJ Web of Conferences 157, 03005 (2017)
[10] M.J. Martin et al. PRL 119, 205002 (2017)
[11] Y Q Yang et al, Plasma Phys. Control. Fusion 59 (2017) 095001
[12] R. Dux Journal of Nuclear Materials 390–391 (2009) 858
[13] B. Lipschultz, D.A. Pappas, B. LaBombard et al, Nucl. Fusion 41, p.585 2001
[14] R. Dux et al. Journal of Nuclear Materials 363–365 (2007) 112–116
[15] L. Zhang et al 2015 Rev Science Instruments, 123509
[16] Z. Xu et al 2018 Nucl. Fusion 58 016001
[17] H. Mao et al. Nuclear Materials and Energy 12 (2017) 447–452
[18] M. H. Li et al. Physics of Plasmas 23, 102512 (2016)
[19] Qin Chengming - Plasma Science and Technology, Vol.17, No.2, Feb. 2015
[20] Zhang et al. Rev. Sci. Instrum. 86, 123509 (2015)
[21] S. Wukitch et al APS Division of Plasma Physics Meeting 2014 DPPUO3012W
[22] V. Bobkov et al., Nuclear Materials and Energy 12 (2017) 1194–1198
[23] K. K. Kirov - Plasma Phys. Control. Fusion 51 (2009) 04400
[24] E. Lerche et al AIP Conference Proceedings 1187, 93 (2009)
[25] V Bobkov et al 2017 Plasma Phys. Control. Fusion 59 014022
[26] Chen Z, Zhao YP, Chen G. et al. NUCL SCI TECH (2018) 29 19
[27] S. Wukitch et al Journal of Nuclear Materials 390–391 (2009) 951–954
[28] R. Perkins et al EPJ Web of Conferences 157, 03039 (2017)